

See discussions, stats, and author profiles for this publication at: <http://www.researchgate.net/publication/50906944>

# Dynamics and control of the two-pulse protocol in electroporation: Numerical exploration

ARTICLE *in* MATHEMATICAL BIOSCIENCES · MARCH 2011

Impact Factor: 1.3 · DOI: 10.1016/j.mbs.2011.03.013 · Source: PubMed

---

READS

23

## 2 AUTHORS:



Wen Jiang

Huazhong University of Science and Technol...

14 PUBLICATIONS 112 CITATIONS

SEE PROFILE



Xiaopeng Zhao

University of Tennessee

80 PUBLICATIONS 597 CITATIONS

SEE PROFILE

# Dynamics and Control of the Two-pulse Protocol in Electroporation: Numerical Exploration

Wen Jiang and Xiaopeng Zhao

September 17, 2011

## Abstract

Externally applied voltages can create transient, nonselective pores in a cell's membrane, a phenomenon known as electroporation. Electroporation has reduced toxicity, is easy to perform, and does not induce the immune system. Therefore, the technique has a wide range of biological and medical applications. Previous experiments show that a two-pulse protocol, which consists of a fast, large-magnitude pulse and a slow, small-magnitude pulse, can increase the efficiency of drug delivery such as gene electrotransfer. In this work, we investigate the dynamics and control of the two-pulse protocol using a macroscopic model of electroporation. Numerical simulations show that there exists a range of pore radii that cannot be sustained using the conventional, open-loop, two-pulse protocol. As a result, one may need to use pores that are significantly larger than the sizes of the targeted molecules. Moreover, it is not possible to know the rate of delivery a priori. To ensure accurate drug delivery and avoid potential damage to the cell's membrane, we explore feedback mechanisms to eliminate the gap in sustainable pore radii and thus to precisely control the electroporation process. Numerical simulations show that a straightforward feedback algorithm can achieve robust control effects. Moreover, the control algorithm is effective without knowledge of the model and thus has the potential to be implemented in experiments.

## 1 INTRODUCTION

Electroporation, also termed electroporabilization, is used to describe the appearance of pores in artificial or cellular membranes, due to an elevated transmembrane voltage caused by an applied electric field [1, 28, 43]. Transport of small molecules such as sucrose, dyes, and monovalent or divalent ions across cell membranes was reported in as early as 1980s [45]. The pores of the electroporated erythrocyte membranes were observed directly using electron microscopy, which suggested that the pores take the shape of an “inverted volcano”—a conical depression with a hole at the bottom [9].

Electroporation has reduced toxicity and is easy and cheap to perform. Moreover, electroporation can be repeated as often as desired since it does not induce the immune system [7, 4]. With these merits, electroporation is now regarded as a useful technique which has many potential medical applications [5, 11, 6, 25]. Of particular interest is *in vivo* gene electrotransfer, which can enhance gene expression by 100- to 1000-folds and has become one of the most efficient non-viral gene transfer methods [2, 3, 4, 7, 15, 27]. Electric pulses can help muscle cell permeabilization and support the migration of DNA toward or across the permeabilized membrane. A two-pulse protocol, consists of two pulses separated by a break interval (see Figure 1), was first proposed by Sukharev et al. [37] for gene delivery applications. Recently, extensive experiments have been conducted to show that the combination of permeabilizing short high-voltage pulses (HV) and electrophoretic long low-voltage pulses (LV) is more efficient for gene electrotransfer in various tissues [37, 34, 32, 3, 13, 19].

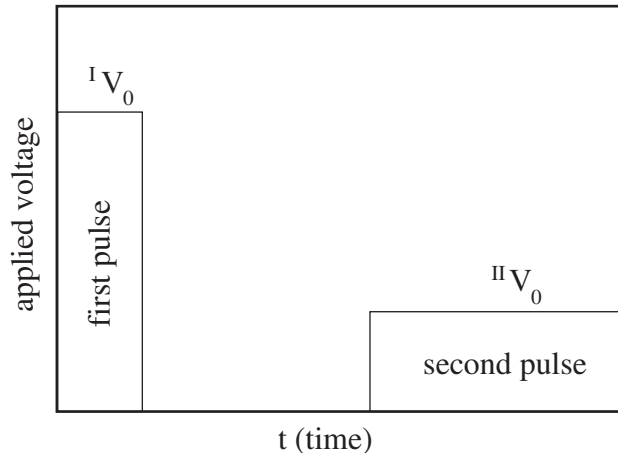


Figure 1: Schematic of a two-pulse protocol.

The mechanisms of electroporation and the two-pulse protocol are still not fully understood [44, 13]. The development of theoretical models of electroporation has lagged behind the experimental research. Molecular dynamics and coarse grain simulations [39, 8, 20, 17] are probably the most promising approaches that are able to offer the most detailed and most accurate description of the process. When coupled with the calculation of electric field distribution of the tissue, these models permit the design and optimization of *in vivo* clinical electroporation protocols. But the size of the system that can be simulated is still rather limited [39, 40]. On the other hand, macroscopic models have provided considerable successes in reproducing the creation and evolution of pores [35, 14, 20] as well as in predicting the spatial distributions of the electric potential, pore density, etc. [30, 24, 16]. Macroscopic models have also been used to optimize the efficiency of electroporation through the control of electric field [23, 38].

In this work, we explore the dynamics and control of the two-pulse protocol of electroporation based on analyses and simulations of a macroscopic model. We first demonstrate limitations of the conventional two-pulse protocol. Specifically, we show that there exists a range of pore radii that cannot be maintained using the conventional two-pulse protocol, which was also implied by experimental work [3]. As such, one may need to use pores that are significantly larger than necessary to deliver certain particles, which in turn may cause damage to a cell's membrane. We investigate the dynamics of pore evolution to understand the mechanisms that lead to these limitations. Then, we explore feedback control mechanisms to eliminate the gap in sustainable pore radii. Numerical simulations show that a straightforward feedback algorithm can achieve robust control effects. Moreover, the control algorithm is model independent and thus has the potential to be implemented in experiments.

## 2 Mathematical Description

Many models of electroporation have been developed by various authors [35, 20, 14, 30, 24, 16]. Despite differences in their mathematical representations, these models are built on similar basic ideas including pore creation energy and conductance of individual pores [44]. In this work, we investigate dynamics and control of electroporation using the model of Smith et al. [35], which was previously verified by Vasikoski et al. [42]. Considering a simple, uniformly polarized membrane, the model of Smith et al. can predict the creation and evolution of large, stable, and reversible pores on the cell membranes due to the external voltage. More recently, this model has been extended to describe electroporation in a spherical cell [26].

During electroporation, all pores are hydrophobic when they are first created [1, 43, 44]. Although most of these pores are quickly destroyed by lipid fluctuations, those, whose radii are greater than a minimum radius  $r_*$ , spontaneously convert to long-lived, hydrophilic pores, which immediately expand to the minimum-energy radius  $r_m$  [31]. Therefore, Smith et al. [35] assumed that all pores are created with the initial radius  $r_m$ . Denote the pore density by  $N$ . The creation rate of pores is described by the following equation [35, 26]:

$$\frac{dN}{dt} = \alpha e^{(V_m/V_{ep})^2} \left( 1 - \frac{N}{N_0 e^{(r_m V_m / r_* V_{ep})^2}} \right), \quad (1)$$

where  $\alpha$  is the creation rate coefficient,  $V_m$  represents the transmembrane potential,  $V_{ep}$  represents the characteristic voltage of electroporation, and  $N_0$  is the equilibrium pore density for  $V_m = 0$ .

Assume there exist  $K$  pores at time  $t$  and denote the radii of these pores by  $r_j$ ,  $j = 1, 2, \dots, K$ . The rates of change of these pores are governed by the following equation [35,

26]:

$$\frac{dr_j}{dt} = -\frac{D}{k_B T_a} \left( -4\beta \frac{r_*^4}{r_j^5} + 2\pi\gamma - 2\pi r_j \sigma_{eff} - \frac{F_{max}}{1 + \frac{r_h}{r_j + r_t}} V_m^2 \right), \quad j = 1, 2, \dots, K, \quad (2)$$

where  $D$  is the diffusion coefficient of the pore radius,  $k_B$  is the Boltzman constant,  $T_a$  is the absolute temperature, and  $\sigma_{eff}$  is the tension of a membrane with pores. The four terms in the parenthesis in Eqn. (2) account for the effects of steric repulsion of lipid heads, the edge energy of the pore perimeter, the effect of pores on the membrane tension, and the contribution of the transmembrane potential, respectively. Note that  $\sigma_{eff}$  is a function of area of pores  $A_s$  [35, 26]:

$$\sigma_{eff} = 2\sigma' - \frac{(2\sigma' - \sigma_0)}{(1 - A_s/A)^2}, \quad (3)$$

where  $A_s = \sum_{j=1}^K \pi r_j^2$ . The physical interpretations and values of other parameters are listed in Table 1.

To account for the influence of the presence of pores on the transmembrane voltage, one needs to specify the type of experimental preparation. The model of Smith et al. considers a simple, uniformly polarized membrane, which can be represented as a circuit with capacitance  $C = C_m A$ , resistance  $R = R_m/A$ , and current  $I_p$ . Here,  $C_m$ ,  $R_m$ , and  $A$  are surface capacitance, surface resistance, and total area of the membrane, respectively. Then, the transmembrane voltage  $V_m$  evolves as follows [35, 26]:

$$\frac{dV_m}{dt} = \frac{1}{C} \left( \frac{V_0}{R_s} - \left( \frac{1}{R_s} + \frac{1}{R} \right) V_m - I_p \right), \quad (4)$$

where  $V_0$  represents voltage,  $R_s$  represents the series resistance of the experimental setup and  $I_p$  is the sum of current through all pores with pore resistance  $R_p = h/(\pi g r^2)$  and input resistance  $R_i = 1/(2gr)$ :

$$I_p = \sum_{j=1}^K \frac{V_m}{R_p(r_j) + R_i(r_j)}. \quad (5)$$

The model Smith et al. have been simplified by a few authors [10, 46] using a two-pulse protocol, where the first pulse create a number of pores of various radii. These authors assume that, pores created in the first phase all shrink to the minimum size  $r_m$  during the break, and moreover application of the second pulse will not change the number of pores. Therefore, all the pores in the second phase have the same radius in this stage. Under this assumption, the dynamics for the second phase can be significantly simplified. Specifically, the number of pores  $K$  becomes a constant and the  $K$  equations in Eqn. (2) become one identical equation as follows:

$$\frac{dr}{dt} = -\frac{D}{k_B T_a} \left( -4\beta \frac{r_*^4}{r^5} + 2\pi\gamma - 2\pi r \left( 2\sigma' - \frac{2\sigma' - \sigma_0}{(1 - \frac{K\pi r^2}{A})^2} \right) - \frac{F_{max}}{1 + \frac{r_h}{r + r_t}} V_m^2 \right). \quad (6)$$

Symbol	Definition	Value
$V_{ep}$	Characteristic voltage of electroporation	0.258 V
$N_0$	Equilibrium pore density at $V_m = 0$	$1.5 \times 10^9 \text{ m}^{-2}$
$\alpha$	Creation rate coefficient	$1.0 \times 10^9 \text{ m}^{-2} \text{ s}^{-1}$
$C_m$	Surface capacitance of the membrane	$9.5 \times 10^{-3} \text{ Fm}^{-2}$
$A$	Total area of lipid bilayer	$1.26 \times 10^{-9} \text{ m}^2$
$R_s$	Series resistance of the experimental setup	100 $\Omega$
$R_m$	Surface resistance of the membrane	$0.523 \Omega \text{ m}^2$
$h$	Membrane thickness	$5 \times 10^{-9} \text{ m}$
$g$	Conductivity of the solution	$2 \text{ Sm}^{-1}$
$D$	Diffusion coefficient for pore radius	$5 \times 10^{-14} \text{ m}^2 \text{ s}^{-1}$
$k_B$	Boltzmann constant	$1.38 \times 10^{-23} \text{ m}^2 \text{ kgs}^{-2} \text{ K}^{-1}$
$T_a$	Absolute temperature	310K
$\beta$	Steric repulsion energy	$1.4 \times 10^{-19} \text{ J}$
$\gamma$	Edge energy	$1.8 \times 10^{-11} \text{ Jm}^{-1}$
$r_h$	Constant for electric force	$0.97 \times 10^{-9} \text{ m}$
$r_t$	Constant for electric force	$0.31 \times 10^{-9} \text{ m}$
$r_m$	Minimum energy radius at $V_m = 0$	$0.8 \times 10^{-9} \text{ m}$
$r_*$	Minimum radius of hydrophilic pores	$0.51 \times 10^{-9} \text{ m}$
$F_{\max}$	Maximum electric force for $V_m = 1 \text{ V}$	$0.7 \times 10^{-9} \text{ NV}^{-2}$
$\sigma_0$	Bilayer tension without pores	$1.0 \times 10^{-3} \text{ Jm}^{-2}$
$\sigma'$	Hydrocarbon water interface tension	$2.0 \times 10^{-2} \text{ Jm}^{-2}$

Table 1: Parameters of the electroporation model.

Moreover, Eqn. (4) is reduced to the following form:

$$\frac{dV_m}{dt} = \frac{1}{C} \left( \frac{V_0}{R_s} - \left( \frac{1}{R_s} + \frac{1}{R} \right) V_m - \frac{KV_m}{R_p(r) + R_i(r)} \right). \quad (7)$$

If the number of pores  $K$  is determined, one can then analyze the dynamics of the second pulse using Eqns. (6,7).

Cranford et al. [10] carried out detailed numerical studies of Eqns.(6,7). They demonstrated that this system possesses bifurcations that lead to bistabilities and discontinuous jumps in pore radius under continuous variation of  $V_0$ . Zhao et al. [46] designed a feedback control algorithm to successfully eliminate the bifurcations and to maintain originally unstable pore radius. Although their control algorithm is rigorous and robust, the control relies on detailed knowledge of the mathematical model. Motivated by the success of the previously developed model-dependent control mechanism, we explore model-independent control algorithms using the more realistic macroscopic model.

## 3 Results

### 3.1 Response of the Two-pulse Protocol

The two-pulse protocol, as sketched in Figure 1, has been proved to be more efficient than a single pulse especially in the uptake of DNA [37, 34, 32, 3]. Using Eqns.(1,2,4), we study evolutions of the pore radii during a two-pulse protocol; see Figure 2. Here, voltage of the first pulse is  $^I V_0 = 1.2\text{V}$ , which lasts for  $20\mu\text{s}$ . During the first pulse, 7468 pores are created, where the maximum radius is 48.8nm, the minimum radius is 0.847nm, and the average radius is 45.7nm. Then, we remove the voltage so that the pores will shrink, which lasts for  $50\mu\text{s}$ . At the end of shrinkage, the radii of all pores reduce to the minimum size  $r_m$ . Finally, the pores expand to and stay at an equilibrium value 28.3nm for the duration of the second pulse, where  $^{II} V_0 = 0.5\text{V}$ .

#### 3.1.1 Influence of the Magnitude of the Second Pulse

It is then interesting to investigate how the pore radius depends on the magnitudes of the two pulses as well as on the duration of the shrinkage. We first study the influences of the magnitude of the second pulse when keeping the other parameters constant. Figure 3 shows the dependence of the equilibrium pore radius on the magnitude of  $^{II} V_0$ . Here, when  $^{II} V_0$  is less than 0.46V, the equilibrium pore radius is no more than 1.2nm. On the other hand, when  $^{II} V_0$  is larger than 0.47V, the equilibrium pore radius is larger than 27.4nm and the equilibrium value monotonically increases as a function of  $^{II} V_0$ . Therefore, pores in the range between 1.2nm and 27.4nm cannot be sustained. Moreover, this gap in sustainable pore radii also depends on the magnitude of  $^I V_0$ . For example, the numerical results for a few selected values of  $^I V_0$  are shown in Table 2.

First pulse $^I V_0$ (V)	Number of pores K	Unsustainable pore radii (nm)
1.15	5105	1.2-33.1
1.20	7468	1.2-27.4
1.25	18144	1.2-17.4
1.30	48550	1.2-10.0

Table 2: Unsustainable pore radii under the two-pulse protocols. The first pulse of  $^I V_0$  is applied for  $20\mu\text{s}$ , then a  $50\mu\text{s}$  breakage is applied before the second pulse, cf. Figure 3.

In nonlinear dynamics, such a tremendous jump in a system's response under a minimal variation in the system's parameters is typically induced by bifurcation [36, 29]. Indeed, Cranford et al. [10] and Zhao et al. [46] showed that the conventional two-pulse protocol is associated with saddle-node bifurcations [36, 29], which lead to jumps in the achievable pore radii. It is interesting to note that this jump phenomenon has been observed in experiments. For example, Andre et al. recently investigated the efficiency of high-

and low-voltage pulse combinations for gene electrotransfer in muscle, liver, tumor, and skin [3]. They studied the dependence of the expression of luciferase gene in rat skin on the low-voltage (LV) electric field strength. When the LV strength is less than 80V/cm, the luciferase activity is on the level of a few pg/mg tissue whereas when the LV strength is greater than 80V/cm, the luciferase activity is increased by an order of magnitude; see Figure 6(a) in [3]. Motivated by the numerical and experimental observations, we will explore feedback algorithms to eliminate the jump phenomena.

### 3.1.2 Influence of the Lag Time

Experiments show that the efficiency of DNA transfection depends on the lag time between HV and LV [3, 34]. Particularly, when the lag time is too short, the efficiency of DNA transfection will decrease. To investigate this issue, we study the model of Smith et al. using a two-pulse protocol with various lag times. In these studies, we choose  $^I V_0 = 1.2V$  and  $^{II} V_0 = 0.4V$ . Numerical simulations show interesting phenomena. When the lag time is sufficiently long, all pores will reduce to the value of  $r_m$  during the shrinkage and all pores increase size simultaneously during the LV pulse (second pulse). However, when the lag time is not sufficiently long, only a part of the pores shrink to  $r_m$ , which will subsequently remain at the radius of  $r_m$  during the second pulse. In contrast, the other pores will increase their radii during the second pulse. Figure 4 shows the evolutions of the maximum, minimum, and average pore radii when the lag time is 40  $\mu s$ . During the second pulse, although the average pore radius is kept to be 25.5nm, the majority of the pores (5327 out of all 7468 pores) remain at the radius of  $r_m$ . Since only a fraction of the pores possess radii that are sufficiently large for molecules to pass, the efficiency of over all drug delivery is expected to be reduced. This behavior provides a potential explanation on the previous experimental observation that reduced lag time leads to decreased efficiency in DNA transfection [3, 34]. Therefore, a sufficient shrinkage time between HV and LV is needed to increase the efficiency of the process. However if the breakage time is too long, pores may start to reseal, which may in turn reduce the efficiency [37].

## 3.2 Design of Feedback Control Algorithms

The gaps in the sustainable pore radii during the conventional two-pulse protocol impose great limitations in practical applications. For example, to admit supercoiled DNA molecules, the pores should be at least 10nm in diameter and last for more than 1 millisecond [33]. On the other hand, toxicity can be reduced if the duration and the level of permeabilization are minimized [7]. However, because of the existence of the range of unsustainable pore radii (see Table 2), one may have to use pores, whose sizes are much larger than necessary. Oversized pores increase the potential of tissue damage. In this section, we investigate feedback control algorithms to enhance the two-pulse protocol by eliminating the gap in sustainable pore radii.

### 3.2.1 Control of Pore Radius

Zhao et al. [46] developed a control mechanism based on a two-dimensional approximation of the model of Smith et al. [35]. They calculated a control input from the model to achieve a targeted pore radius. Although the control is robust and effective, one needs to know the detailed formula of the model. The simplified model is based on an assumption that the second pulse does not create new pores. While the assumption is valid when the magnitude of the second pulse is sufficiently low, it may not be accurate when the magnitude becomes large. Here, we extend that work by considering model-independent controls that are based on feedback of measured quantities. Moreover, the control is implemented in the full model of Smith et al. [35], which is impossible using the original model-dependent control algorithm.

First, we note that the open-loop electroporation process exhibits hysteresis phenomena under quasi-static loading and unloading processes [46]. To manifest, we again apply  $I V_0 = 1.2\text{V}$  for  $20\mu\text{s}$  followed by a break of  $60\mu\text{s}$ . Then, we choose the second pulse to be  $II V_0 = 0.4 + 0.2\sin(1000t)$ , simulating a slow loading and unloading process. Figure 5 shows the hysteresis loop during the loading and unloading process. It is clear that the hysteresis loop in the  $r$ - $V_0$  space is an envelope of the  $r$ - $V_0$  shown in Figure 3. Now, suppose we want to maintain the pore radius at an arbitrary value  $r_{\text{target}}$ . We first choose  $V_{\text{max}}$  to be a value above the top envelope in Fig. 5 and  $V_{\text{min}}$  be a value below the bottom envelope in Figure 5. We intend to design a control algorithm that can adjust the external voltage  $V_0$  according to the following feedback rules:

$$II V_0 = \begin{cases} V_{\text{max}} & \text{if } r < r_{\text{target}} - r_{\text{error}} \\ V_{\text{min}} + \frac{V_{\text{max}} - V_{\text{min}}}{2r_{\text{error}}}(r_{\text{target}} + r_{\text{error}} - r) & \text{if } |r - r_{\text{target}}| \leq r_{\text{error}} \\ V_{\text{min}} & \text{if } r > r_{\text{target}} + r_{\text{error}} \end{cases} . \quad (8)$$

It is clear that this control algorithm will drive the pore radius to and maintain in the range of  $|r - r_{\text{target}}| \leq r_{\text{error}}$ . Moreover, since the feedback relation intersects the  $r$ -nullcline in this range to result an equilibrium, this feedback algorithm is able to maintain the pore radius at a constant within the error range. As examples, we apply the control algorithm in Eqn. (8) to acquire pore radii at  $r_{\text{target}} = 10$  and  $25\text{nm}$ , respectively. For purpose of illustration, we choose  $V_{\text{max}} = 0.7\text{V}$ ,  $V_{\text{min}} = 0\text{V}$  and  $r_{\text{error}} = 0.1\text{nm}$ . Figure 6 shows that the controlled pore radii approach  $10.001\text{nm}$  and  $24.998\text{nm}$ , respectively. It is important to note that the pore radius monotonically approaches the targeted value, which is in contrast to the normal limit-cycle behaviors in typical PID controllers [21, 12].

### 3.2.2 Control of DNA Transfection Rate

Although the control of pore radius is successful, one shall note that it is not possible to directly measure the radii of pores in real-time experiments. As an alternative, one could consider to control the transfer rate of the delivered molecules. To demonstrate the principles, we consider the DNA transfection rate in gene electrotransfer experiments.

According to Neumann et al. [30], the uptake of the DNA is described by the Nernst-Planck equation, which accounts for both the diffusive and electrophoretic transport:

$$\frac{d[\text{DNA}]_{\text{in}}}{dt} = -\frac{D_0}{hV_{\text{cell}}}A_s(t) \times \left( [\text{DNA}]_{\text{in}} - [\text{DNA}]_{\text{out}} \left( 1 + \frac{|z_{\text{eff}}|e}{k_B T_a} V_m(t) \right) \right), \quad (9)$$

where  $[\text{DNA}]_{\text{in}}$  and  $[\text{DNA}]_{\text{out}}$  are concentrations of DNA inside and outside the cell, respectively,  $D_0$  is the DNA diffusion coefficient,  $V_{\text{cell}}$  is the volume of the spherical cell with a  $10\mu\text{m}$  radius,  $z_{\text{eff}}$  is the effective valence of the DNA molecule, and  $e$  is the elementary charge. We choose values of those parameters following the reason mentioned by Smith et al. [35]. The values of parameters are listed in Table 3. The uptake for DNA is divided by two to account for the fact that negatively charged DNA molecules enter predominantly through the depolarized half of the cell [22]. When the pore radius is less than 10nm, the rate of DNA transport  $\frac{d[\text{DNA}]_{\text{in}}}{dt} = 0$ . We design a control mechanism that can adjust the external voltage  ${}^{II}V_0$  according to the following feedback rules:

$${}^{II}V_0 = \begin{cases} V_{\text{max}} & \text{if } \frac{d[\text{DNA}]_{\text{in}}}{dt} = 0 \\ V_{\text{prev}} + K_p \left( \frac{d[\text{DNA}]_{\text{in}}}{dt} - [\text{DNA}]_{\text{target}} \right) & \text{if } \frac{d[\text{DNA}]_{\text{in}}}{dt} > 0 \end{cases}. \quad (10)$$

Symbol	Definition	Value
$D_0$	DNA diffusion coefficient	$1.3 \times 10^{-12} \text{m}^2/\text{s}$
$[\text{DNA}]_{\text{out}}$	Concentration of DNA outside the cell	$1.3 \times 10^{-6} \text{mol}/\text{m}_3$
$z_{\text{eff}}$	Effective valence of the DNA molecule	-27
$e$	Elementary charge	$1.60217646 \times 10^{-19} \text{C}$

Table 3: Parameters of the model of DNA uptake.

As is shown in Figure 7, we choose  ${}^{II}V_0 = V_{\text{max}}$  when the rate of DNA uptake is zero (i.e., the pore radius is less than 10nm) and apply a simple P control with  $K_p = 0.01V \cdot s$  when the pore radius is larger than 10nm to maintain the rate of DNA transport at the level of 50/s. Finally the pore radius is about 12.1nm and the external voltage is about 0.295V. For practical applications in experiments, the choice of control parameters, such as  $V_{\text{max}}$  and  $K_p$ , shall be determined by properties of the specific system. There is no “one set of parameters fits all.” A rule of thumb in choosing  $V_{\text{max}}$  is 1.) to conduct a quasi-static loading and unloading study to produce a hysteresis loop like the one shown in Figure 5; and 2.) to choose  $V_{\text{max}}$  to be a value above the top envelope. The choice of  $K_p$  requires some trial and error investigations and may be limited by experimental conditions.

## 4 Discussion

Various experiments have demonstrated that the two-pulse protocol is more efficient in gene transfer [37, 34, 32, 3]. Previous numerical studies on a simplified model show that there exists a jump in the sustained pore radii when the magnitude of the low-voltage pulse is gradually increased [10, 46]. Most interestingly, this jump phenomenon has been also observed in experiments. For example, Andre et al. show a discontinuous change in the expression level of luciferase gene in rat skin when the strength of the low-voltage pulse is increased; see Figure 6(a) in [3].

Motivated by these observations, we have explored dynamics and control of the two-pulse protocol in electroporation. First, we have shown that there exists a range of pore radii that cannot be maintained using the conventional two-pulse protocol, which may be the underlying reason for the observed jump in the gene expression activity in the experiments of Andre et al. [3]. Second, numerical simulations show that the decrease in transfection efficacy of DNA under reduced lag time [3, 34] may be caused by the decrease of the number of effective pores. Moreover, we have explored model-independent control algorithms to eliminate the jumps in sustainable pore radii as well as in transfer rates of drug delivery. Unlike conventional model-based controls, the control algorithm developed here utilizes dynamic characteristics of electroporation. The control algorithm is robust: it works for any targeted pore radius no matter the solution is originally stable or unstable. More importantly, the present control algorithm does not require explicit knowledge of the underlying model and can be extended to other measurable variables such as the rate of DNA uptake. Therefore, the control algorithm can be easily applied to other models.

There exist many practical challenges to implement the proposed control algorithms in experiments. First, pore radii can not be directly measured in real-time experiments. Measurement of drug transfer rate is also difficult. For example, experiments have demonstrated that permeation of fluorescent-labeled DNA can be observed at the frequency of 1 Hz [47, 19]. Nevertheless, successful implementation of the control algorithms described here would require real-time measurement and regulation on the order of microsecond, the characteristic time of electroporation dynamics. In electroporation experiments, external voltage can not be directly measured or adjusted. Instead, voltage is related to electric field strength and the distance. Thus, in a wet lab, control can be implemented by adjusting either electric field strength or the distance. While the current manuscript demonstrates the effectiveness of control using voltage, in practice, the control algorithm can be implanted using other tunable parameters. Moreover, the current study is based on a macroscopic model developed by Smith et al. [35]. The results need to be further verified using other models. Since the existing macroscopic models of electroporation are built on similar basic ideas including pore creation energy and conductance of individual pores [44], we suspect similar phenomena happen in other macroscopic models. Nevertheless, to fully understand the mechanisms underlying jump phenomena, one may have

to resort to detailed studies using molecular dynamics simulations.

## Acknowledgements

This work is in part supported by the NSF under grant No. CMMI-0845753. The authors are also grateful to Wanda Krassowska Neu for her insightful discussions. We thank the anonymous reviewers for their invaluable comments, which have helped to improve the quality of this article.

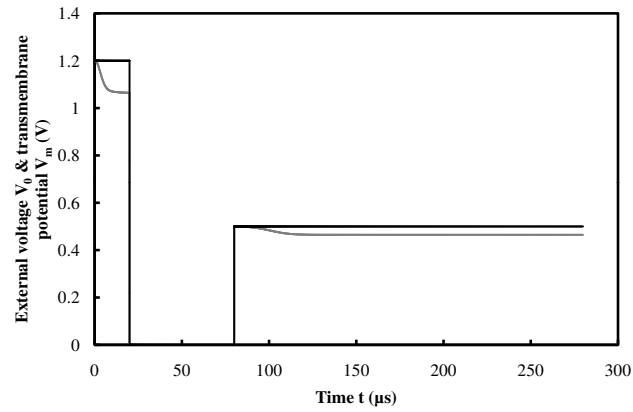
## References

- [1] I. G. Abiror, V. B. Arakelyan, L. V. Chernomordik, Y. A. Chizmadzhev, V. F. Pastushenko, and M. R. Tarasevich. *Electric breakdown of bilayer lipid membranes I. The main experimental facts and their qualitative discussion*, Bioelectrochemistry and Bioenergetics, **6** (1979), 37–52.
- [2] H. Aihara, and J. Miyazaki. *Gene transfer into muscle by electroporation in vivo*, Nat. Biotech., **16** (1998), 867–870.
- [3] F. M. Andre, J. Gehl, G. Sersa, V. Preat, P. Hojman, J. Eriksen, M. Golzio, M. Cemazar, N. Pavselj, M. -P. Rols, D. Miklavcic, E. Neumann, J. Teissie, and L. M. Mir. *Efficiency of high- and low-voltage pulse combinations for gene electrotransfer in muscle, liver, tumor, and skin*, Hum. Gene Ther., **19** (2008), 1261–1271.
- [4] FM Andre, LM Mir, *Nucleic Acids Electrotransfer In Vivo: Mechanisms and Practical Aspects*, Current Gene Therapy, **10** (2010), 267-280.
- [5] P.F. Baker, D. E. Knight. *A high-voltage technique for gaining rapid access to the interior of secretory cells*, J.Physiol., **284** (1978), 30–31.
- [6] R. Benz, F. Beckers, U. Zimmerman. *Reversible electrical breakdown of lipid bilayer membranes: a charge pulse relaxation study*, J. Membr. Biol., **48** (1979), 181–204.
- [7] P. Bigey, M. F. Bureau and D. Scherman. *In vivo plasmid DNA electrotransfer*, Curr. Opin. Biotechnol., **13** (2002), 443–447.
- [8] RA Boeckmann, BL de Groot, S Kakorin, *Kinetics, statistics, and energetics of lipid membrane electroporation studied by molecular dynamics simulations*, Biophysical Journal, 95 (2008), 1837-1850.
- [9] D. C., Chang, *Structure and dynamics of electric field-induced membrane pores as revealed by rapid-freezing electron microscopy*, in “ Guide to Electroporation and

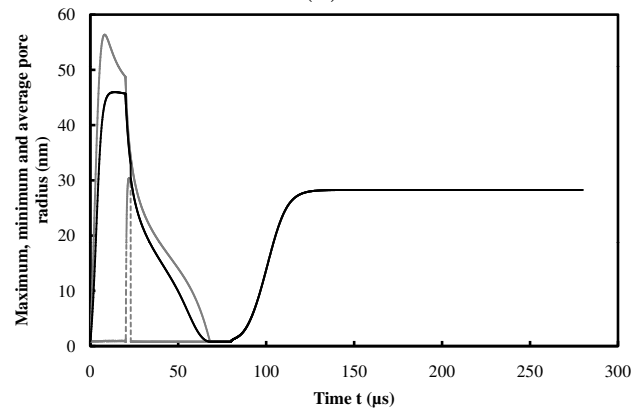
- Electrofusion ” (eds. D.C. Chang, B.M. Chassy, J.A. Saunders, and A.E. Sowers), Academic, San Diego, CA, (1992), 9–27.
- [10] J. P. Cranford, X. Zhao, and W. Krassowska. *Guidelines for controlling pore radii from nonlinear analysis of a two dimensional model of electroporation*, in “ASME International Mechanical Engineering Congress and Exhibition ” , Seattle, Washington, (2007), 10-16.
- [11] S.B. Dev, D. P. Rabussay, G. Widera, and G. A. Hofmann. *Medical applications of electroporation*, IEEE Trans. on Plasma Science, **28** (2000), 206–223.
- [12] R. C. Dorf, and R. H. Bishop. “Modern Control Systems ”, Prentice Hall, 2005.
- [13] J. M. Escoffre, T. Portet, L. Wasungu, J. Teissie, D. Dean, M.-P. Rols. *What is (still not) known of the mechanism by which electroporation mediates gene transfer and expression in cells and tissues* , Mol. Biotechnol., **41** (2009), 286–295.
- [14] S. A. Freeman, M. A. Wang, and J. C. Weaver. *Theory of electroporation of planar bilayer membranes: predictions of the aqueous area, change in capacitance, and pore-pore separation*, Biophys. J., **67** (1994), 42–56.
- [15] J. Gehl. *Electroporation: theory and methods, perspectives for drug delivery, gene therapy and research* , Acta physiologica Scandinavica, **177** (2003), 437–447.
- [16] T. R. Gowrishankar, and J. C. Weaver. *An approach to electrical modeling of single and multiple cells* , Proc Natl Acad Sci USA, **100** (2003), 3203–3208.
- [17] AA Gurtovenko, I Vattulainen, *Calculation of the electrostatic potential of lipid bilayers from molecular dynamics simulations: Methodological issues*, JOURNAL OF CHEMICAL PHYSICS, **130** (2009), 215107.
- [18] Times Cited: 3
- [19] A. Hassibi, H. Vikalo, J. L. Riechmann and B. Hassibi. *Real-time DNA microarray analysis* , Nucleic Acids Res., doi:10.1093/nar/gkp675, (2009).
- [20] R. P. Joshi, and K. H. Schoenbach. *Electroporation dynamics in biological cells subjected to ultrafast electrical pulses: A numerical simulation study*, Phys. Rev. E, **62** (2000), 1025–1033.
- [21] H. K. Khalil. “Nonlinear Systems ”, Prentice Hall, 2002.
- [22] V. A. Klenchin, S. I. Sukharev, S. M. Serov, L. V. Chernomordik, and Y. A. Chizmadzhev. *Electrically induced DNA uptake by cells is a fast process involving DNA electrophoresis* , Biophys. J., **60** (1991), 804–811.

- [23] T. Kotnik, L. M. Mir, K. Flisar, M. Puc and D. Miklavcic. *Cell membrane electroporation by symmetrical bipolar rectangular pulses: Part I. Increased efficiency of permeabilization*, Bioelectrochem., **54** (2001), 83–90.
- [24] T. Kotnik, and D. Miklavcic. *Theoretical evaluation of voltage inducement on internal membranes of biological cells exposed to electric fields*, Biophys. J., **90** (2006), 480–491.
- [25] W. Krassowska. *Effects of electroporation on transmembrane potential induced by defibrillation shocks*, Pacing Clin. Electrophysiol., **18** (1995), 1644–1660.
- [26] W. Krassowska, and P. D. Filev. *Modeling electroporation in a single cell*, Biophys. J., **92** (2007), 404–417.
- [27] J. McMahon and D. Wells. *Electroporation for gene transfer to skeletal muscles: current status*, BioDrugs, **18** (2004), 155–165.
- [28] L. M. Mir, S. Orłowski, J. Belehradec, J., and C. Paoletti. *Electrochemotherapy potentiation of antitumour effect of bleomycin by local electric pulses*, Eur. J. Cancer, **27** (1991), 68–72.
- [29] A. H. Nayfeh, and B. Balachandran. “Applied Nonlinear Dynamics”, New York: Wiley, 1995.
- [30] Neumann, E., S. Kakorin, I. Tsoneva, B. Nikolova, and T. Tomov. *Calcium-mediated DNA adsorption to yeast cells and kinetics of cell transformation by electroporation*, Biophys. J., **71** (1996), 868–877.
- [31] J. C. Neu, and W. Krassowska. *Asymptotic model of electro-poration*, Phys. Rev. E, **59** (1999), 3471–3482.
- [32] N. Pavšelj, V., Pr eat. *DNA electrotransfer into the skin using a combination of one high- and one low-voltage pulse*, J. Control. Release, **106** (2005), 407–415.
- [33] V. V. Rybenkov, A. V. Vologodskii, and N. R. Cozzarelli. *The effect of ionic conditions on the conformations of supercoiled DNA, Sedimentation analysis*, J. Mol. Biol., **267** (1997), 299–311.
- [34] S. Satkauskas, M. F. Bureau, M. Puc, A. Mahfoudi, D. Scherman, D. Miklavcic, and L. M. Mir. *Mechanisms of in vivo DNA electrotransfer: respective contributions of cell electroporation and DNA electrophoresis*, Mol. Ther., **5** (2002), 133–140.
- [35] K. C. Smith, J. C. Neu and W. Krassowska. *Model of creation and evolution of stable electropores for DNA delivery*, Biophys. J., **86** (2004), 2813–2826.

- [36] S. H. Strogatz. “ Nonlinear Dynamics and Chaos: With Applications to Physics, Biology, Chemistry, and Engineering ”, Addison-Wesley Publishing Company , 1994.
- [37] S. I. Sukharev, V. A. Klenchin, S. M. Serov, L. V. Chernomordik, and YuA Chizmadzhev. *Electroporation and electrophoretic DNA transfer into cells: The effect of DNA interaction with electropores* , Biophys. J., **63** (1992), 1320–1327.
- [38] S. Talele, and P. Gaynor. *Non-linear time domain model of electropermeabilization: Response of a single cell to an arbitrary applied electric field* , J. Electrostat., **65** (2007), 775–784.
- [39] M. Tarek. *Membrane electroporation: A molecular dynamics simulation* , Biophys. J., **88** (2005), 4045–4053.
- [40] D. P. Tieleman. *The molecular basis of electroporation* , BMC Biochem., **5** (2004), 10–21.
- [41] D. P. Tieleman, and S. J. Marrink. *Lipids out of equilibrium: Energetics of desorption and pore mediated flip-flop* , J. Am. Chem. Soc., **128** (2006), 12462–12467.
- [42] Z. Vasikoski, A. T. Esser, T. R. Gowrishankar, and J. C. Weaver *Membrane electroporation: The absolute rate equation and nanosecond time scale pore creation* , Phys. Rev. E, **74** (2006), 021904(12).
- [43] J. C. Weaver. *Electroporation: a general phenomenon for manipulating cells and tissues* , J. Cell. Biochem., **51** (1993), 426–435.
- [44] J. C. Weaver. *Electroporation of biological membranes from multicellular to nano scales* , IEEE Trans. Dielectr. Electr. Insul., **10** (2003), 754–768.
- [45] U. Zimmermann, J. Vienken, and G. Pilwat. *Development of drug carrier systems: electrical field induced effects in cell membranes* , Bioelectrochem Bioenerg, **7** (1980), 553–574.
- [46] X. Zhao, M. Zhang and R. Yang. *Control of pore radius regulation for electroporation-based drug delivery* , Commun Nonlinear Sci Numer Simul. DOI: 10.1016/j.cnsns.2009.05.059,(in press).
- [47] Z. Zhu, J. Chao, H. Yu and A. S. Waggoner. *Directly labeled DNA probes using fluorescent nucleotides with different length linkers* , Nucleic Acids Res., **22** (1994), 3418–3422.



(a)



(b)

Figure 2: Response to a two-pulse protocol: (a) evolution of external voltage (solid black) and transmembrane potential (solid grey); and (b) evolution of maximum (solid grey), average (solid black), and minimum (dash grey) pore radii. Note that during the second pulse, all pores have the same radius. The first pulse of 1.2 V is applied for  $20\mu\text{s}$ . Then, after a  $60\mu\text{s}$  break, a second pulse of 0.5 V is applied for  $200\mu\text{s}$ .

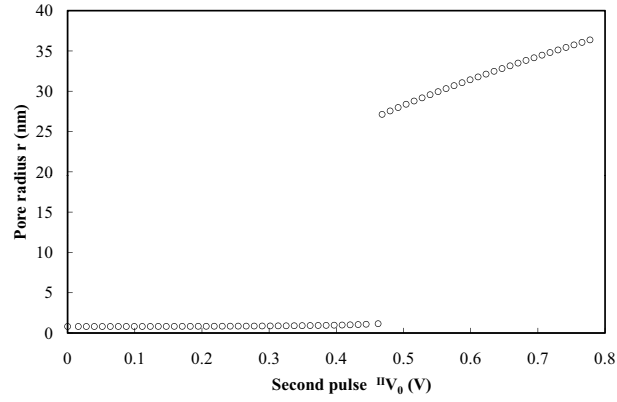


Figure 3: Dependence of the equilibrium pore radius on the magnitude of  ${}^{II}V_0$  in the second pulse of a two-pulse protocol. Note that the second pulse is preceded by a first pulse with  ${}^I V_0 = 1.2\text{V}$ .

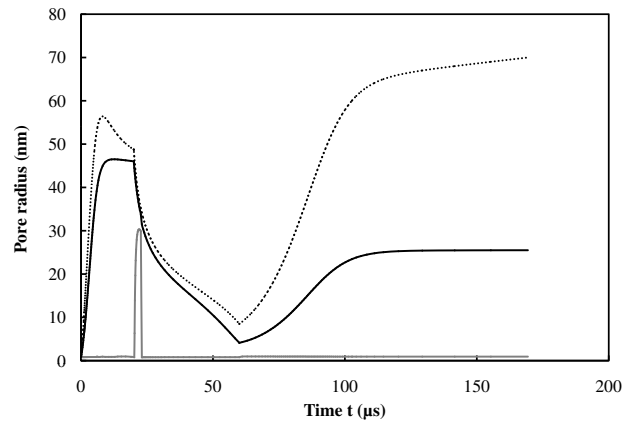


Figure 4: The influence of lag time between HV and LV on the pore radius: maximum radius (black dash), average radius (black solid) and minimum radius (grey solid).

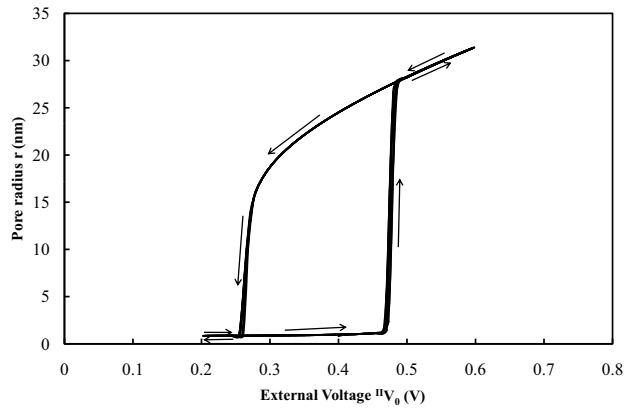
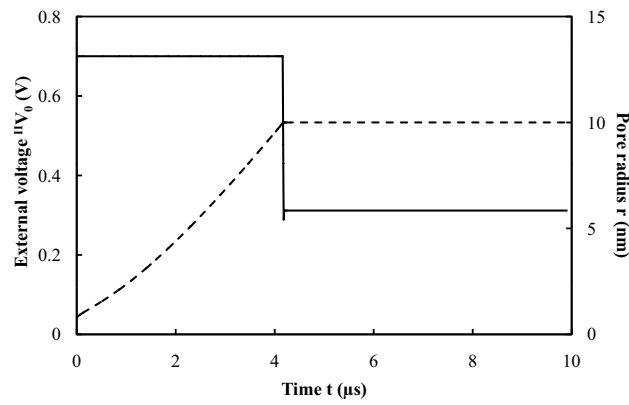
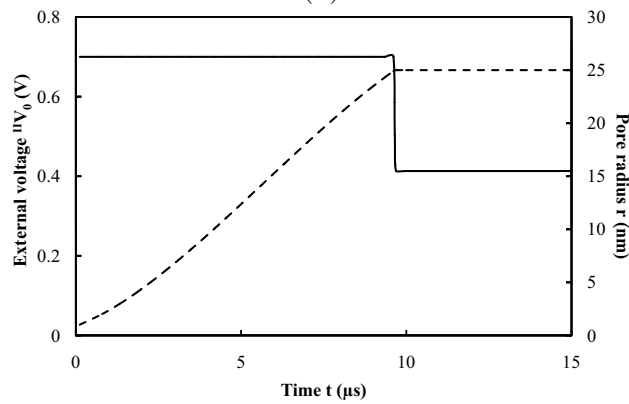


Figure 5: Hysteresis under a quasi-static loading and unloading process.

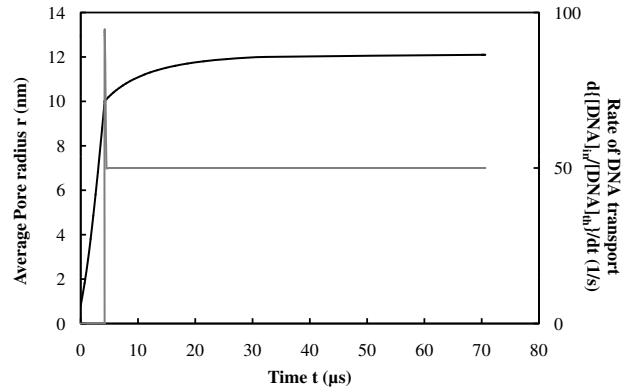


(a)

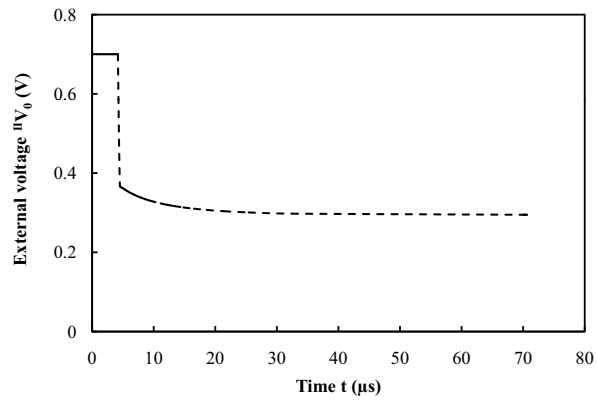


(b)

Figure 6: Controlled response based on model independent algorithm with targeted radius (a) 10nm; (b) 25nm: response of  $r$  (dashed) and response of  $V_0$ .



(a)



(b)

Figure 7: Controlled response based on the rate of DNA uptake (50/s): Evolution of (a) the rate of DNA transport (grey solid) and pore radius (black solid); (b) the external voltage (black dash) during the control period.